



Anodized titania nanotube array microfluidic device for photocatalytic application: Experiment and simulation

Harikrishnan Jayamohan ^a, York R. Smith ^{b,*}, Lauryn C. Hansen ^b, Swomitra K. Mohanty ^c, Bruce K. Gale ^a, Mano Misra ^{b,c, **}

^a Department of Mechanical Engineering, University of Utah, Salt Lake City, UT 84112, USA

^b Department of Metallurgical Engineering, University of Utah, Salt Lake City, UT 84112, USA

^c Department of Chemical Engineering, University of Utah, Salt Lake City, UT 84112, USA



ARTICLE INFO

Article history:

Received 22 October 2014

Received in revised form 25 February 2015

Accepted 27 February 2015

Available online 2 March 2015

Keywords:

Anodization

Titania nanotubes

Photocatalysis

Microfluidic reactors

Simulation

ABSTRACT

Microfluidic photocatalytic reactors have advantages over conventional bulk reactors such as large surface-area-to-volume ratio and high control of fluid flow. Although titania nanotubular arrays (TNA) have shown enhanced photocatalytic degradation compared to nanoparticle films in a batch reactor configuration, their application in a microfluidic format has yet to be explored. The photocatalytic performance of a microfluidic reactor with TNA catalyst was compared with the performance of microfluidic format with TiO₂ nanoparticulate (commercial P25) catalyst. The microfluidic device was fabricated using non-cleanroom based soft lithography, making it suitable for economical large scale manufacturing. The photocatalytic performance was evaluated at different flow rates ranging from 25 to 200 μL/min. The TNA microfluidic system demonstrated enhanced photocatalytic performance over microfluidic TiO₂ nanoparticulate layers, especially at higher flow rates (50–200 μL/min). For instance, 12 μm long TNA was able to achieve 82% fractional conversion of 18 mM methylene blue in comparison to 55% conversion in case of the TiO₂ nanoparticulate layer at a flow rate of 200 μL/min. A computational model of the microfluidic format was developed to evaluate the effect of diffusion coefficient and rate constant on the photocatalytic performance. The improved performance of the TNA photocatalyst over the nanoparticle film can be attributed to higher generation of oxidizing species.

© 2015 Elsevier B.V. All rights reserved.

1. Introduction

Water based pollutants are a big concern and serious challenge in both developed and developing nations. Photocatalytic environmental remediation has been widely investigated for the degradation of water based pollutants [1]. Recently, nanomaterials such as nanoparticles, nanowires and nanoporous films have been applied to photocatalytic reactions due to their interesting properties over bulk materials. Many studies have used photocatalysts in the form of a powder. However, the use of powdered photocatalysts necessitates their downstream recovery, which can be costly. The immobilization or growth of photocatalysts as a film eliminates this drawback. Many studies involve conventional macroscale reactors

with limited mass transport and poor photon transport. This can potentially limit the degradation performance of the system [2–4]. The use of microfluidic system has the potential to reduce such aforementioned reactor limitations.

Microfluidic systems have inherent advantages such as large surface to volume ratio, smaller diffusion distance, uniform irradiation over the whole catalytic surface, self-refreshing property [5] and large mass transfer efficiency [6,4]. Microfluidic photocatalytic reactors have demonstrated higher photocatalytic efficiency compared to conventional reactors. For example, Lei et al. reported reaction rate constants in microreactors to be 100 times more than in bulk reactors [3]. In bulk reactors, there is a loss of photons reaching the photocatalyst surface due to scattering effects in the liquid [7]. In contrast, in microfluidic reactors, the thin layer of liquid over the catalyst ensures that less photons are lost due to scattering. Microfluidic reactors can also be used for rapid screening of photocatalysts [4,8].

Of the semiconductor materials studied for photocatalytic environmental remediation, titanium dioxide (e.g., nanoparticle, nanowires, nanotubes) is widely used due to its desirable

* Corresponding author. Tel.: +1 801 581 6386; fax: +1 801 581 4937.

** Corresponding author at: Department of Metallurgical Engineering, University of Utah, Salt Lake City, UT 84112, USA. Tel.: +1 801 581 6386; fax: +1 801 581 4937.

E-mail addresses: york.smith@utah.edu (Y.R. Smith), mano.misra@utah.edu (M. Misra).

properties. Titanium dioxide has successfully demonstrated photocatalytic degradation of a wide spectrum of metallic and organic pollutants [9]. Titania nanotube arrays (TNA) synthesized by anodization have received interest in last few decades in areas such as sensing, drug-delivery, energy conversion/storage, and catalysis, for example [10–12]. Macak et al. reported the use of high-aspect ratio TNA for enhanced photocatalytic properties compared to TiO_2 nanoparticulate layers [13]. Although the TNA layer was five times shorter than the P25 nanoparticulate layer, it still exhibited enhanced photocatalytic performance compared to the latter. In their study, the photocatalytic experiments were performed in a batch reactor configuration. Most of the current literature on photocatalytic microfluidic systems involve TiO_2 nanoparticle film as a photocatalyst [14,15,3,16,17]. Subsequently, a more efficient degradation system could be realized by integrating TNA in a microfluidic system. Moreover, microfluidic devices integrated with TNA can potentially be used for other applications such as photocatalytic syntheses of chemicals such as L-pipecolinic acid, for example [18].

A potential disadvantage with current microfluidic photocatalytic degradation systems is that the microfluidic devices needed are often complex and difficult to fabricate especially when clean-room techniques are involved. This is especially critical when a large-scale array of microfluidic channels is required [4]. For example, previous reports on microfluidic photocatalytic devices used clean-room techniques to fabricate the mold for the microfluidic device [14,3,6] or to pattern the photocatalyst substrate [2] or CNC milling to pattern the substrate [19]. In contrast, in this study the microreactor mold was fabricated using laser patterned polymethyl methacrylate (PMMA) sheets [20,21] and polydimethylsiloxane (PDMS) was used to fabricate the device. A widely used material for microfluidic devices, PDMS, has desirable properties such as optical transparency, chemical inertness, and easy and rapid fabrication [22,17].

In this work, we demonstrate the use of self-ordered TNA for photocatalytic degradation in a microfluidic reactor. The degradation performance of TNA was also compared to P25 TiO_2 nanoparticle films in a similar microfluidic format. The degradation kinetics of a model pollutant (methylene blue) in a microfluidic channel with TNA vs. P25 TiO_2 particles as catalyst under solar irradiation (AM 1.5, $\sim 100 \text{ mW/cm}^2$) was used in this study. Most of the existing work on microfluidic photocatalytic system, however, have been done under UV light [2,6,17], limiting the practical application.

We have also developed a model using COMSOL Multiphysics to examine how convection and diffusion of the reactant/pollutant molecules affect the performance of the microfluidic surface reactor system. Although models have been developed to understand the nature and reaction kinetics between a photocatalyst and reactant in batch reactors [23–26], a model that would explain the behavior of such a system in a microfluidic flow based scenario has yet to be explored.

2. Experimental

2.1. Preparation and characterization of TNA and P25 film

Titania nanotube arrays were synthesized by electrochemical anodization similar to an earlier reported protocol [27,28]. In short, Ti foils (0.02032 cm thick) were cut into $3 \text{ cm} \times 2 \text{ cm}$ and anodized under sonication (Branson 5510 ultrasonic bath) in an electrolytic solution consisting of ethylene glycol (Fisher Scientific, Waltham, MA), deionized (DI) water (2 wt.%) and ammonium fluoride (0.5 wt.%, Fischer Scientific) at 30°C bath temperature. One side of the Ti foil was masked using Kapton tape to restrict oxide

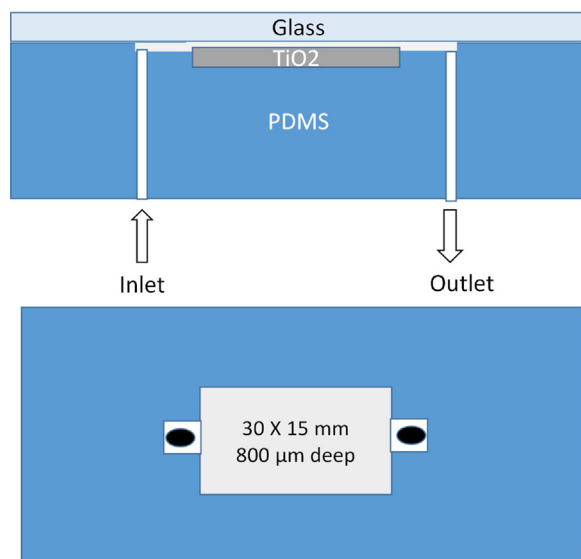


Fig. 1. Top and side view of the microfluidic device.

growth to only one side of the Ti strip. A two electrode configuration with platinum (Pt) mesh as the cathode was used for anodization. The anodization was carried out at an applied potential of 60 V(D.C.) (Agilent, E3647A) for different time intervals (60 min for long tubes, 30 min for medium tubes and 15 min for short tubes). The thus formed TNA were rinsed with DI water, air-dried and cut to the dimension of the microfluidic channel. The TNA samples were subsequently annealed in an atmosphere of N_2/H_2 (2% H_2) at 500°C ($1.6^\circ\text{C}/\text{min}$ ramp rate) for 2 h.

The P25 films were prepared by doctor blade method [29]. A fine paste of Degussa P25 was made with dilute nitric acid (pH 3–4) using a mortar and pestle. Scotch tape (3M) was used as a mold to form a film the same dimensions of the channel ($30 \text{ mm} \times 15 \text{ mm}$) on a Ti foil. Subsequently the P25 film was calcined in air for 2 h at 450°C . The morphology of the thus formed P25 TiO_2 and TNA films were characterized using a field emission scanning electron microscope (SEM) (Hitachi, S-4800). The crystalline properties of the films were examined using X-ray diffraction (Rigaku MiniFlex 600) with $\text{CuK}\alpha$ radiation ($\lambda = 0.1542 \text{ nm}$) from $2\theta = 20\text{--}80^\circ$ with a step size = 0.01° and dwell time = $0.5^\circ/\text{min}$.

2.2. Fabrication of microfluidic channel and integration of TNA substrate

The microfluidic device was fabricated by soft lithography similar to a previous procedure [30]. A laser was used to create the mold for the microfluidic channel on a PMMA sheet ($800 \text{ }\mu\text{m}$ thick) and transferred onto a plastic petri dish. The dimensions of the channel are as shown in Fig. 1. A 20 mL mixture of PDMS (base to curing agent ratio – 1:10) was poured onto the mold and cured at 60°C for 4 h to create the PDMS layer. Subsequently, inlet and outlet channels were bored onto the PDMS channel. Then the thin film catalyst (TNA or P25 film) was embedded (using a double-sided tape) into the PDMS channel. The TNA or P25 layer was placed facing the glass slide. The glass slide was bonded to the PDMS layer via corona surface treatment for 4 min and subsequently baked at 60°C for 2 h [31].

2.3. Evaluation of the photocatalytic degradation

The photocatalytic degradation of the device was evaluated using methylene blue (MB) as a model pollutant. This dye is non-biodegradable and commonly used in the textile industry. As

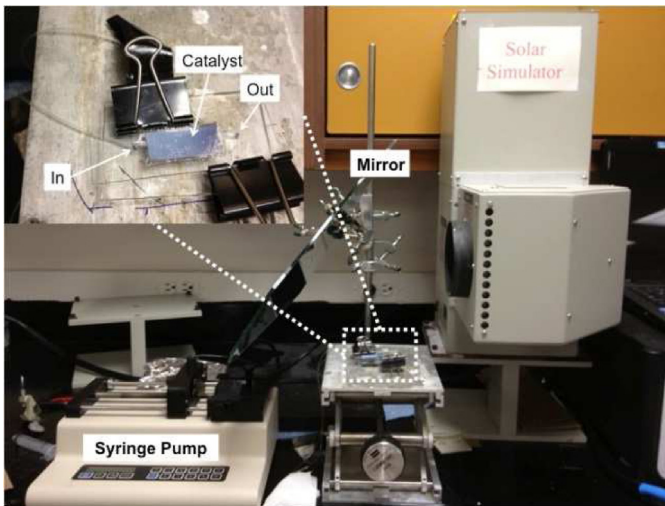


Fig. 2. Experimental setup used for microfluidic photodegradation of MB. The inset shows the actual microfluidic reactor with the TNA catalyst embedded.

a result, this molecule is widely used for testing photocatalytic activity [32,33,13]. A depiction of the experimental setup used to evaluate the photocatalytic performance is shown in Fig. 2. In a typical experiment run, 5 mL of 18 mM aqueous solution of MB was injected through the inlet into the microfluidic device using a syringe pump (KD Scientific, Manassas, VA) via Tygon tubing (0.02 in. inner diameter) at different flow rates ranging from 25 to 200 $\mu\text{L}/\text{min}$. The microfluidic device was irradiated with AM 1.5 simulated solar light. The intensity of the light was measured at the surface of the microfluidic device using a handheld power meter (Nova, Ophir-Spiricon, UT) to be $\sim 100 \text{ mW}/\text{cm}^2$. The syringe pump was used to flow 1 mL of the MB solution through the device with the simulated solar light irradiation before any sample was collected. This was to ensure steady state is reached before the MB degradation is measured. The degraded MB solution was collected and the concentration was analyzed by monitoring the decrease in characteristic absorption peak at $\lambda = 664 \text{ nm}$ using a UV-vis spectrophotometer (Shimadzu Corp., Japan). The fractional conversion (X) was calculated by:

$$X = \frac{A_0 - A}{A_0} \quad (1)$$

where A_0 is the initial concentration absorbance value, and A is the absorbance value of the degraded solution. The experiment was repeated in the absence of AM 1.5 light to evaluate the amount of MB adsorbed on the catalyst. All photocatalytic degradation experiments were repeated 3–5 times and the fractional conversion values averaged. Error bars on all plots are $\pm \sigma$ of the experimental data.

3. Numerical modeling

A finite element model to simulate the degradation of MB in the microfluidic channel was created in COMSOL Multiphysics 4.3b. For simplicity, the model assumes the catalytic surface to be a flat surface rather than nano-structured. The model also assumes that the bulk MB solution is transported to the catalyst surface at the bottom of the channel and degraded.

3.1. Microchannel geometry

Fluid flows using 3-D model geometries were developed. Fig. 3 shows the geometry of the 3-D model used in the simulations. The x and y dimensions of the channel match the geometry of the

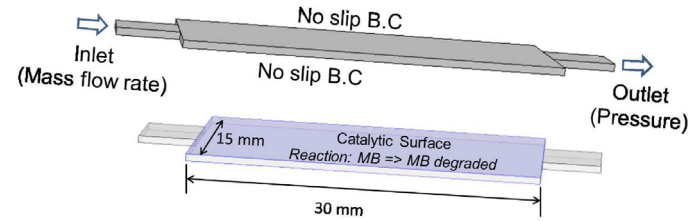


Fig. 3. Boundary conditions used in simulation of the 3D model.

microchannel fabricated for the experiments. The z dimension is assumed to be 600 μm . This is because the overall height of the channel is 800 μm and the thickness of the Ti foil/catalyst layer is approximated as 200 μm .

3.2. Fluid flow

The Navier–Stokes equations for conservation of momentum (2) and the continuity equation for conservation of mass (3) are used to model the laminar flow of a single phase Newtonian fluid in the micro-channel.

$$\rho \left(\frac{\partial \vec{u}}{\partial t} \right) + \vec{u} \cdot \nabla \vec{u} = -\nabla p + \mu \nabla^2 \vec{u} \quad (2)$$

$$\rho \nabla \vec{u} = 0 \quad (3)$$

In Eqs. (2) and (3), u is the flow velocity field, μ is the dynamic viscosity of the fluid, ρ is the fluid density and p is the fluid pressure. At the walls of the microfluidic channel, no-slip boundary conditions are applied. Eqs. (2) and (3) assume the system is under steady-state conditions with negligible body forces and uniform fluid density. The inlet fluid mass flow rate was specified and a no-slip boundary is assumed at the channel surfaces. Based on the given boundary conditions the velocity and pressure fields are computed inside the microfluidic channel.

3.3. Species concentration

The equation for convection-diffusion of the species in the fluid is given by (assuming constant diffusion coefficient)

$$\frac{\partial \vec{c}}{\partial t} = -D \nabla^2 \vec{c} + R - \vec{u} \cdot \nabla \vec{c} \quad (4)$$

where c and D are the concentration and the diffusion coefficient of the species, respectively, in a fluid flowing with velocity u and R is the reaction rate in the bulk solution. The diffusion coefficient of MB is assumed to be $1.6 \times 10^{-10} \text{ m}^2/\text{s}$ [34].

3.4. Degradation reaction

The overall degradation of MB happens at the catalytic surface only and not the bulk solution. The boundary fluxes at the catalytic surfaces thus are denoted by

$$R_i = n \cdot (-D_i \delta c_i + c_i u) \quad (5)$$

where the reaction rate $R_i = kc$ and k is the forward reaction rate constant. The model solves for concentration profile of the product (degraded MB) along the channel based on the given flow conditions and reaction parameters.

4. Results and discussion

4.1. Characterization

Figs. 4 and 5 show the SEM image of the annealed TNA of different lengths. The nanotube lengths are approximately 12 μm

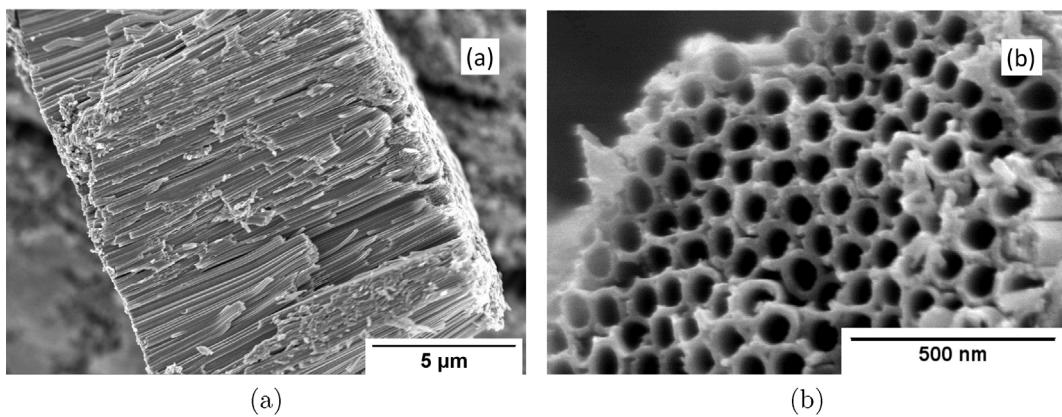


Fig. 4. SEM images of TNA anodized at 60 V for 1 h duration, showing the sidewall morphology (a) and top morphology (b).

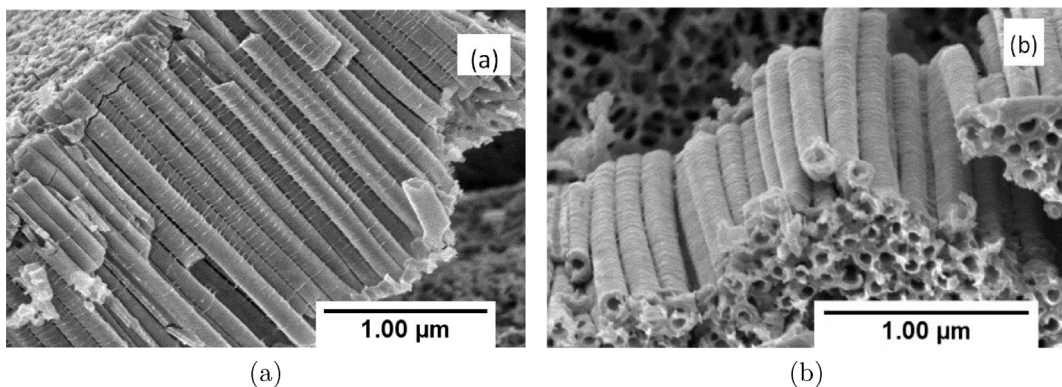


Fig. 5. SEM images of TNA anodized at 60 V for 15 min anodization, showing the sidewall (a) and top morphology (b).

(1 h anodization, **Fig. 4**), 7 μm (30 min anodization – not shown) and 3 μm (15 min anodization, **Fig. 5**). The TNA tubes have an approximate inner diameter of 80 nm with an average wall thickness of 15 nm. In comparison, the TiO_2 P25 layer (**Fig. 6**) has particles and agglomerates of 20–50 nm size with a layer thickness of approximately 40 μm .

The crystalline structure is one of the critical factors in the catalytic performance of TiO_2 at a liquid–solid interface [35,13,36,37]. The XRD patterns of the annealed P25 and TNA catalysts are shown in **Fig. 7**. The diffraction patterns have been indexed to standard JCPDS cards. From the peak positions and the relative intensities, it is evident that both P25 (**Fig. 7a**) and TNA (**Fig. 7b**) contain two titania crystalline phases, anatase (labeled A) and rutile (labeled R).

The underlying titanium support (labeled T) is also evident in both samples. It is evident that the predominant phase is anatase.

4.2. Degradation performance of the microfluidic reactor: effect of flow rate and nanotube length

The results of the degradation at different flow rates over TNA (12 μm) and TiO_2 P25 in the presence and absence of AM 1.5 irradiation are presented in **Fig. 8a**. At the lowest flow rate, both the TiO_2 P25 and 12 μm thick TNA catalysts show similar degradation performance. As the flow rate increases from 50 to 200 $\mu\text{L}/\text{min}$, the fractional conversion of the P25 catalyst decreases from 0.93 to 0.55. In contrast, the TNA fractional conversion remains relatively

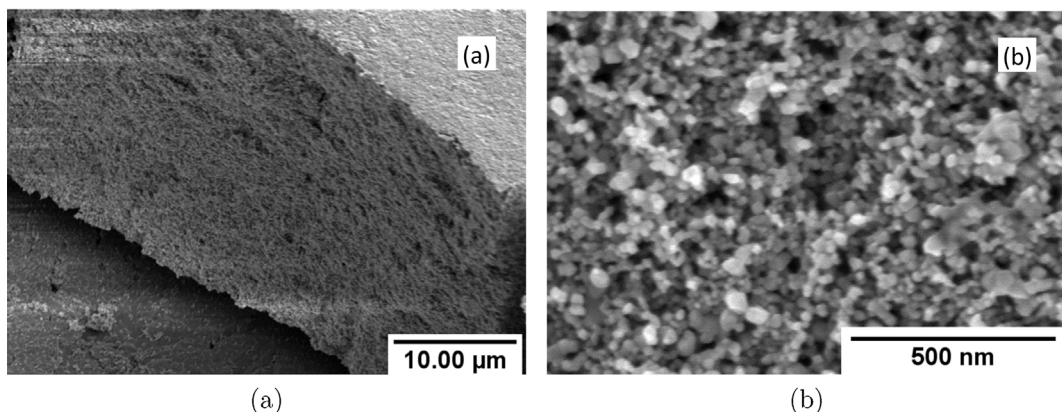


Fig. 6. SEM images of P25 TiO_2 layer prepared by doctor blade method, showing the film sidewall morphology (a) and top morphology (b).

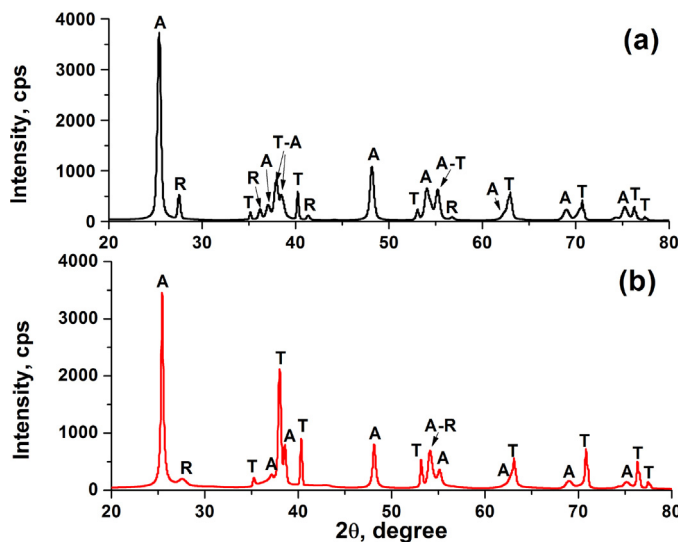


Fig. 7. X-ray diffraction patterns of annealed (a) P25 photocatalyst and (b) 12 μm TNA photocatalyst. For both photocatalysts, both anatase (indexed labeled A) and rutile (index labeled R) crystal phases are identified. The underlying titanium substrate (indexed labeled T) is also identified.

constant over the flow rate range of 50–200 $\mu\text{L}/\text{min}$. The thickness of the TNA and P25 oxide layer has shown to be correlated to the level of degradation performance in batch reactor systems [13]. It is interesting to note that, even though the P25 layer is more than three times as thick (40 μm) as the longer TNA (12 μm), the degradation performance is much higher in the case of 12 μm TNA. The results of the fractional conversion in the absence of AM 1.5 light gives an indication of how much dye is adsorbed on the catalyst. It is observed that the P25 film adsorbs more dye at a flow rate of 25 $\mu\text{L}/\text{min}$ compared to TNA. For higher flow rates, the dye adsorption remains relatively constant and is approximately the same for both P25 and TNA. At the lowest flow rate, the molecules have more time to adsorb and equilibrate with the catalyst surface. The higher dye adsorption on the P25 film compared to the TNA film is possibly due to a larger surface area of the P25 film over the 12 μm TNA film. However, it should be noted that the ability of a dye molecule to adsorb onto a titania surface is predisposed to the surface charge of that catalyst (i.e., isoelectric point) and of the dye molecule [38]. In nanomaterials, this can vary depending upon the synthesis method adopted, polymorph, crystallographic planes, as well as crystallite size [12]. The degradation performance for different lengths of TNA catalyst was also examined (Fig. 8b). The shorter TNA lengths (7 and 3 μm) have a degradation performance lower than that of the P25 film within the flow rate domain. It should be noted, that the decrease in fractional conversion with an increase in flow rate from

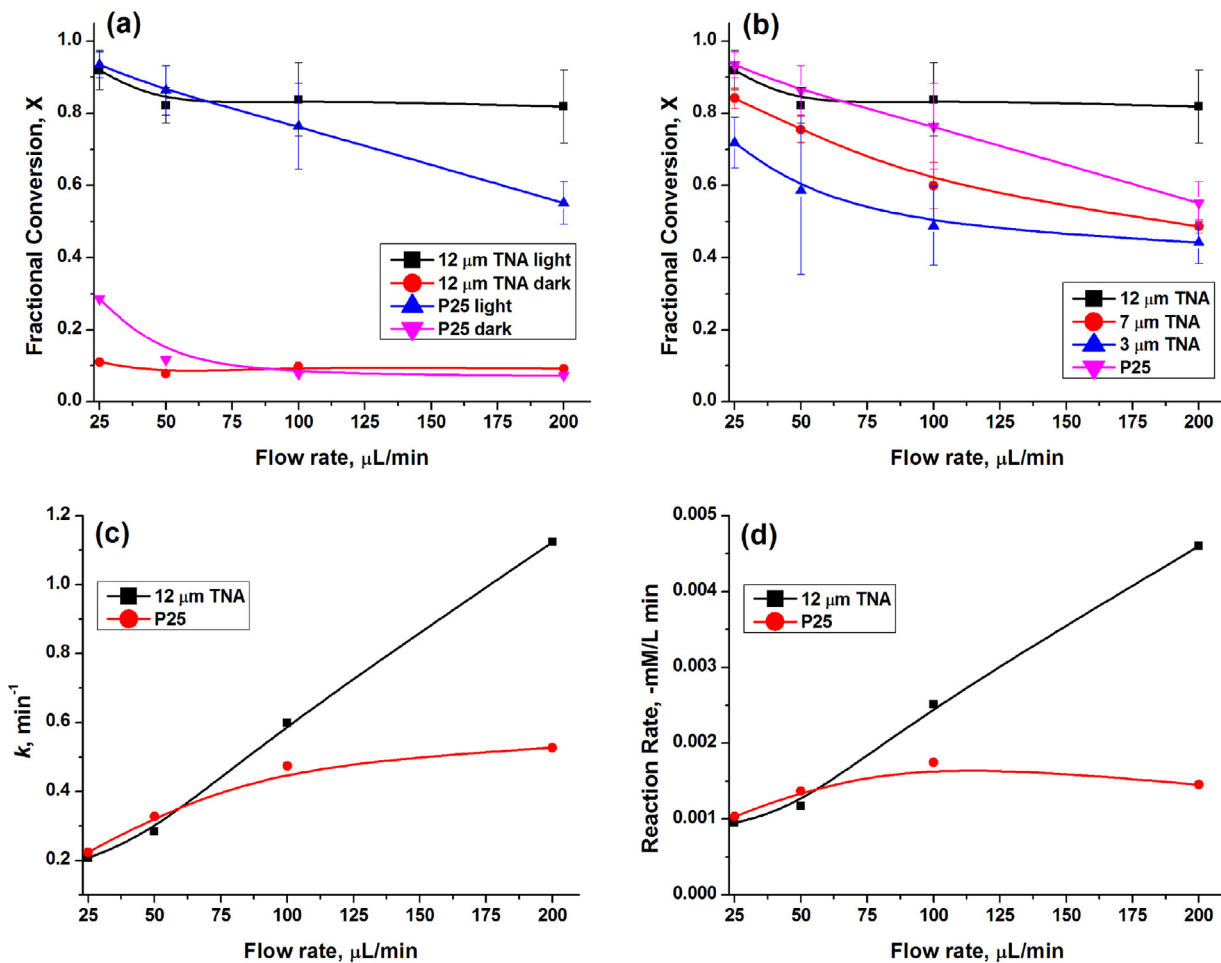


Fig. 8. (a) Effect of flow rate on MB degradation for 12 μm TNA and P25 TiO_2 film catalyst in the presence and absence of AM 1.5 irradiation ($\sim 100 \text{ mW/cm}^2$). (b) Effect of TNA length (12, 7 and 3 μm) on MB degradation at different flow rates under AM 1.5 irradiation ($\sim 100 \text{ mW/cm}^2$). (c) Pseudo-first order rate constant of MB degradation at different flow rates for TNA vs. P25 layer. (d) Reaction rate for photocatalytic MB degradation at different flow rates for TNA vs. P25 layer.

50 to 200 $\mu\text{L}/\text{min}$ for 7 and 3 μm TNA is less than that of the P25 catalyst over the same range.

4.3. Evaluation of photocatalytic degradation

The mechanism for the photocatalytic degradation of MB has been discussed in previous published work [13,39]. In short, the adsorbed MB molecules on the catalyst surface are oxidized by the photoinduced holes of the TiO_2 catalyst to form $\cdot\text{MB}^+$ radicals. These radicals further react with O_2 to form $[\text{MBOO}^{\cdot}]^+$, subsequently the heteropolyaromatic ring is broken and is eventually degraded to mineral acids and CO_2 [39]. However, it should be noted, the degradation mechanism when using P25 under these experimental conditions is likely different than when TNA are used as the photocatalyst. The UV portion of AM 1.5 irradiation is a small contribution; moreover P25 is only UV photoactive. Whereas the synthesis method used to prepare TNA in this study results in doped carbon and sub-stoichiometric titania, which contributes to visible light photoactivity [28,12,40,41]. Visible light photocatalysis is achievable using P25, however the mechanism is different and based on dye/ligand-sensitization phenomena [42,43]. Although the degradation pathway and product distribution may be different for each system, the objective of this study is to examine the overall photoconversion of each system based on flow parameters.

Heterogeneous photocatalytic degradation is not an elementary process, i.e., there are several reaction intermediates; moreover, the reaction intermediate species and/or dissolved oxidizing species can act as catalysts for the degradation of other intermediate species. As a result, the reaction order can change along the reaction coordinate. To overcome such complexities, we can assume that the non-degraded MB is in large excess compared to other degradation products. This is generally an adopted approach when examining the kinetics of photocatalytic reactions and is commonly referred as pseudo-order rate kinetics. Kinetic studies on the photocatalytic degradation of azo dyes using TNA [38] and titania nanoparticle films [44] show that they follow a pseudo first order kinetics, and under certain operating conditions, follow the Langmuir–Hinshelwood mechanism. If we assume that the rate-limiting step is the surface reaction, the concentration of oxidizing species (OH^{\cdot} radicals and holes) is assumed to be in large excess. The reaction rate is then assumed to be proportional to the flow rate or residence time (or dye molecules adsorbed). By assuming plug flow within the microfluidic channel and an isothermal pseudo-first order irreversible reaction, the dye concentration (C_A) can be expressed as:

$$C_A = C_{A0} \cdot e^{-kt} \quad (6)$$

where C_{A0} is the initial dye concentration, k is the pseudo-first order rate constant, and τ is the residence time. The pseudo-first order rate constant and reaction rate as a function of flow rate for 12 μm TNA and P25 photocatalysts were calculated and plotted in Fig. 8c and d. From these plots it is evident that for the TNA photocatalyst, as the flow rate increases the reaction rate and rate constant increase over the entire domain of flow rates. This indicates that the surface reaction occurs fast and the kinetics is diffusion limited over the flow rate domain. For the P25 film, the reaction rate and pseudo-first order rate constant, plateaus at 100 $\mu\text{L}/\text{min}$ and remains constant thereafter, thus for flow rates $>100 \mu\text{L}/\text{min}$, the kinetics for the P25 films is reaction limited. It is worth noting, the range of Reynolds numbers for these flow rates is 0.05–0.4 (for 25–200 $\mu\text{L}/\text{min}$) and is still well within the laminar flow regime (i.e., no turbulent mixing effects). Thus the degradation kinetics can be explained in terms of the diffusion of reacting species, and the photocatalysts ability to suppress charge carrier recombination.

Another possible explanation for the higher fractional conversion at higher flow rates (50–200 $\mu\text{L}/\text{min}$) is that the roughness

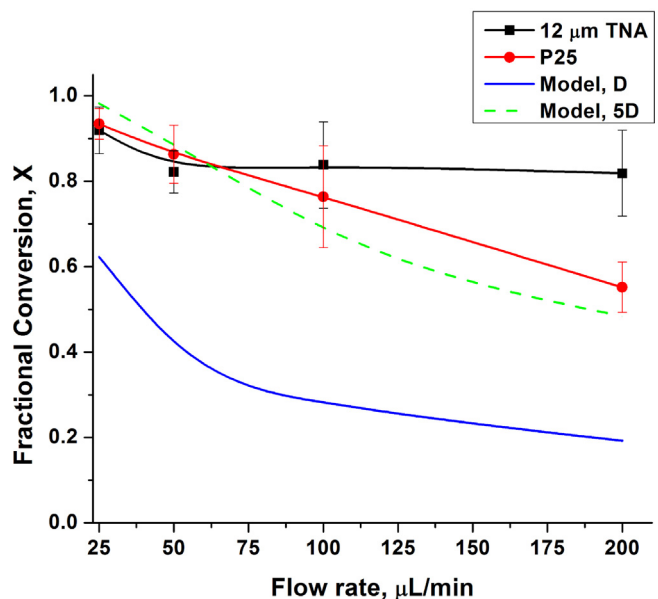


Fig. 9. Results of actual degradation (TNA and P25) in comparison to simulation data for the photocatalytic degradation of methylene blue (18 mM initial concentration). By increasing the diffusion coefficient (D), the simulation data begins to match the experimental data.

might be inducing localized mixing at higher flow rates in the case of TNA. At low Reynolds numbers (<2300) and given a relative roughness of 0.02 (for the TNA layer in this study), the surface roughness does not normally affect the flow in macro systems [45]. But in the case of microfluidic systems, it has been reported that nanoscale surface roughness does cause flow perturbations in low Reynolds number flows ($\text{Re} = 0.06\text{--}6.5$) [46]. The induced flow perturbations could possibly contribute to the mixing of MB and generated oxidizing species, resulting in an enhanced degradation.

Titania nanotube arrays have been reported to have higher photocatalytic efficiency compared to P25 layers in spite of their lower surface area compared to the latter [47]. The TNA nanotubes provide an optimized geometry that has a shorter carrier-diffusion path in the tube walls and lower recombination rates of photo-generated electron–hole pairs in comparison with P25 layer. In the case of P25, the charge carriers have to travel between single nanoparticles, where higher interfacial grain boundaries may lead to increased charge recombination rates. Also, the diffusion path of the dye molecules from bulk solution to the active surface area on a tubular geometry is much shorter compared to the tortuous path in porous structured P25 [48]. Therefore, the enhanced degradation performance of the TNA photocatalyst vs. the P25 photocatalyst may be attributed to better charge separation and diffusion of reacting species.

4.4. Simulation results

The results of the simulation showing fractional conversion of MB in comparison to experimental results (12 μm TNA and P25 catalyst) at different flow rates are shown in Fig. 9. The fractional conversion as per the simulation is lower than what is observed during the experiment for TNA and P25 TiO_2 catalyst (Fig. 8). This may be because the simulation assumes a smooth planar surface, unlike in the case of TNA and P25, which have porous, nanostructured surfaces. Due to the length scales involved, it is computationally expensive to incorporate the exact geometry of a nanostructured surface in the current model. One method to overcome this limitation is to increase the diffusivity of MB to account for the enhanced mass transfer due to a larger surface area and

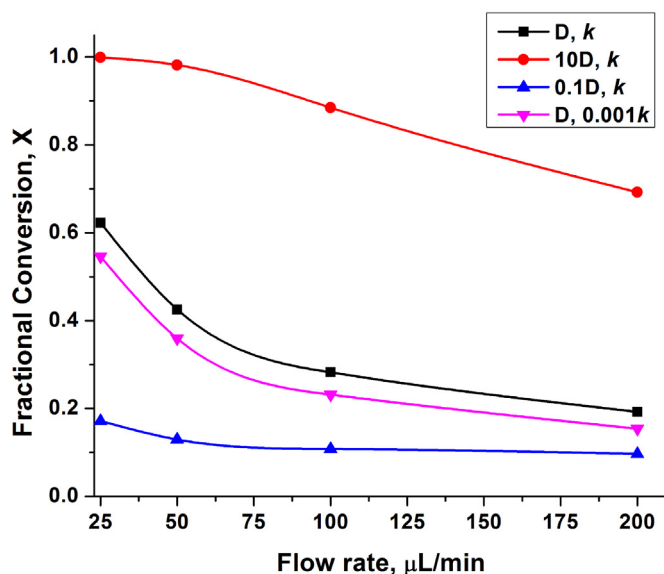


Fig. 10. Simulation on the effect of diffusion coefficient and pseudo-first order rate constant on the degradation of methylene blue. The simulation results are more sensitive to changes in the diffusion coefficient than to the reaction rate constant.

higher number of reactive sites. For example, by increasing the actual diffusion coefficient of MB by five times ($5D$), the simulation results begin to match the experimental results obtained with P25 photocatalyst (Fig. 9).

The better performance of TNA can be attributed to lower recombination rates of photogenerated electron–hole pairs [13]. This can be assumed equivalent to increasing the rate constant. To examine this modeling analog, we have conducted simulations of fractional conversion at different flow rates while varying the diffusion coefficient ($D = 1.6 \times 10^{-10} \text{ m}^2/\text{s}$ for methylene blue [34,49]) and pseudo-first order rate constant ($k = 0.2238 \text{ min}^{-1}$), respectively (Fig. 10). The pseudo-first order rate constant was calculated from experimental results of P25 TiO_2 catalyst at $25 \mu\text{L}/\text{min}$. At this flow rate, the reaction rate and pseudo-first order rate constant are nearly the same for both photocatalysts; moreover, the degradation is least affected by mass transport. It is evident from the simulation that increasing the diffusion coefficient or the rate constant results in increased fractional conversion. It is interesting to note, the effect of rate constant on the fractional conversion is less than that of the diffusion coefficient. For example, reducing the rate constant by three orders of magnitude ($0.001k$) only results in an 18% reduction in fractional conversion at flow rate of $100 \mu\text{L}/\text{min}$. In comparison, a drop in diffusion coefficient by an order of magnitude (D to $0.1D$) resulted in a 62% reduction in fractional conversion at flow rate of $100 \mu\text{L}/\text{min}$. From the results of these simulations the diffusion of reacting species plays a larger role than rate constant.

But an enhancement in diffusion coefficient by five times the actual value seems an unlikely real world scenario even when a nanostructured surface is present. For instance, at a diffusion coefficient of $5D$, it takes 225 s for a MB molecule to diffuse the height of the microfluidic channel. While at a flow rate of $200 \text{ L}/\text{min}$ the MB molecule advects across the length (30 mm) of the channel in 81 s . Hence it is unlikely that during this time period, the MB molecule would diffuse from the bulk to the surface of the TNA catalyst. In the model developed in this study, the assumption is that the MB molecules have to diffuse to the surface of the catalyst to be degraded. An alternate theory can be examined based on diffusion of oxidizing species from surface of the catalyst to the bulk solution. Based on existing work, we know that oxidizing species (OH^\bullet , O_2^\bullet , H_2O_2) are generated at the surface of the TNA catalyst

by reaction of the photogenerated electron–holes in an aqueous solution [50–52,13,53]. While the lifetime of OH^\bullet , O_2^\bullet radicals are very short, hydrogen peroxide (H_2O_2) molecules can remain stable and potentially diffuse from catalyst surface to MB present in solution. For instance, Fujishima reported long-range photocatalytic bactericidal effect (up to $50 \mu\text{m}$) from the surface of TiO_2 films and proposed H_2O_2 and other oxygen species as likely agents [54]. Remote bleaching of methylene blue in gas phase at a distance of $500 \mu\text{m}$ away from the surface of UV irradiated TiO_2 films has been reported [55,52]. With a diffusion coefficient of $1.71 \times 10^{-9} \text{ m}^2/\text{s}$ [56], it would take 26 s for the H_2O_2 molecule to diffuse half the height of the microfluidic channel. We assume the generation of the H_2O_2 and other oxidizing species are limited by their concentration near surface of TNA catalyst. Hence at larger flow rates larger amounts of H_2O_2 molecules are carried away from the catalyst surface by the flow, resulting in a faster generation of H_2O_2 molecules. These molecules could potentially mix with the MB not just in microfluidic channel but also once the sample is collected. This would account for the higher conversion achieved at larger flow rates. Since the height of the TNA array would determine the amount of the oxidizing species generated, the longer the TNA array tubes, the better the degradation performance [13]. This fits well with the results observed in this study for different nanotube lengths (Fig. 8b).

4.5. Degradation performance of the microfluidic reactor – system performance comparison with current literature

The degradation performance of other titania-based photocatalytic microfluidic systems has been compiled and compared (Table 1). Although all of the studies mentioned in Table 1 use methylene blue, it is difficult to compare the performance of TNA photocatalyst with these systems due to the different channel geometries, flow-rates, pollutant concentration and photocatalyst surface area involved. The degradation performance in these systems is reported as a function of irradiation time [2] or the effective residence time [6]. In the case of microfluidic surface reactors, the Péclet number determines whether diffusion or advection is the dominating means of pollutant mass transport to the photocatalyst surface. Hence we have converted the results of these studies as a function of dimensionless Péclet number

$$Pe = \frac{(L \times U)}{D} \quad (7)$$

where L is the characteristic length, U the flow velocity, and D is the mass diffusion coefficient. The Péclet number is a measure of relative importance of advection to diffusion [57,58]. The dimensionless Péclet numbers corresponding to the flow rates 200 , 100 , 50 and $25 \mu\text{L}/\text{min}$ are $8P$, $4P$, $2P$ and P ($P = 9639$). These equivalent Péclet numbers enable comparison with other microfluidic surface reaction systems of varied geometries with the exception for the system reported by Qin et al. [6] (electrospun nanofibrous TiO_2), the maximum Péclet number of the microfluidic systems are less than Péclet numbers for this study ($38,556$). Hence the advection to diffusive mass transport is higher in the microfluidic system in this study compared to the other two studies mentioned. Since the irradiance intensity and wavelength of light source are different for the other studies in Table 1, an absolute degradation performance comparison is not possible. But in terms of comparison based on the nature of convective flow in the microfluidic system, the results of this study demonstrates a much larger advective flow conditions than the other two studies mentioned earlier [3,17]. For instance, the Péclet number defines how rapidly the inlet pollutant is carried by the moving fluid towards the catalyst relative to how fast the degraded products are transferred from the catalyst surface to the center of the fluid flow for removal [59]. Hence the larger the Péclet

Table 1

Summary of reported titania-based photocatalytic microfluidic systems for MB degradation.

Photocatalyst	Irradiance intensity (mW/cm ²)	Wavelength & lamp source	Flow rates (μL/min)	Peclet number range	Initial concentration of MB (M)	Percent conversion reported
TiO ₂ coated fiber glass	2	310–400 nm, 150 W mercury lamp	33.3–200	541–3248	20 × 10 ^{−6}	45–90% [17]
Electrospun nanofibrous TiO ₂	50	365 nm, UV-LED lamp	25–100	20,300–81,198	31 × 10 ^{−6}	55–95% [6]
P25 TiO ₂ film	100	AM 1.5 simulated solar light	150–900	2256–13,533	30 × 10 ^{−6}	48–94% [3]
P25 TiO ₂ film	100	AM 1.5 simulated solar light	25–100	9639–38,556	18 × 10 ^{−3}	55–93% (this study)
TNA	100	AM 1.5 simulated solar light	25–100	9639–38,556	18 × 10 ^{−3}	82–92% (this study)

number, a higher throughput of fluid in the microfluidic system can be realized.

5. Conclusion

The photocatalytic degradation of a model compound, methylene blue, was examined in a microfluidic system using TNA photocatalyst under simulated AM 1.5 irradiation. The microfluidic device was constructed using a non-clean room, inexpensive, rapid prototyping technique. When compared to a film of commercial P25 photocatalyst, TNA demonstrated enhanced degradation over the range of flow rates examined. Analysis of the degradation kinetics reveals that a 12 μm TNA photocatalyst operates under diffusion limited conditions for all flow rates studied, while the P25 photocatalyst film operates under reaction limited conditions at higher flow rates. The improved performance of the TNA photocatalyst over P25 can be attributed to better diffusion of reacting species and improved charge separation. A comparison with other titania-based photocatalytic microfluidic systems reported in the literature based on the dimensionless Pélet number is discussed.

A finite element model was developed to simulate the degradation of MB in the microfluidic channel utilizing COMSOL Multiphysics. From the model developed, the effect of diffusion coefficient and rate constant is discussed. The effect of the diffusion coefficient on the fractional conversion is more sensitive than that of the rate constant. The model can be easily modified to suit other channel geometries, pollutants with different diffusion coefficients, or different values of rate constants.

Acknowledgement

The work presented here was supported by the Utah Science Technology and Research (USTAR) initiative.

References

- H. Lachheb, E. Puzenat, A. Houas, M. Ksibi, E. Elaloui, C. Guillard, J.-M. Herrmann, Photocatalytic degradation of various types of dyes (Alizarin S, Crocein Orange G, Methyl Red, Congo Red, Methylene Blue) in water by UV-irradiated titania, *Appl. Catal. B: Environ.* 39 (1) (2002) 75–90.
- Z. Han, J. Li, W. He, S. Li, Z. Li, J. Chu, Y. Chen, A microfluidic device with integrated ZnO nanowires for photodegradation studies of methylene blue under different conditions, *Microelectron. Eng.* 111 (2013) 199–203.
- L. Lei, N. Wang, X. Zhang, Q. Tai, D.P. Tsai, H.L. Chan, Optofluidic planar reactors for photocatalytic water treatment using solar energy, *Biomicrofluidics* 4 (4) (2010) 043004.
- L. Helen, et al., Microfluidic reactors for photocatalytic water purification, *Lab Chip* 14 (6) (2014) 1074–1082.
- N. Wang, X. Zhang, B. Chen, W. Song, N.Y. Chan, H.L. Chan, Microfluidic photoelectrocatalytic reactors for water purification with an integrated visible-light source, *Lab Chip* 12 (20) (2012) 3983–3990.
- Z. Meng, X. Zhang, J. Qin, A high efficiency microfluidic-based photocatalytic microreactor using electrospun nanofibrous TiO₂ as a photocatalyst, *Nanoscale* 5 (11) (2013) 4687–4690.
- A. Kar, Y.R. Smith, V. Subramanian, Improved photocatalytic degradation of textile dye using titanium dioxide nanotubes formed over titanium wires, *Environ. Sci. Technol.* 43 (9) (2009) 3260–3265.
- H. Zhang, J.-J. Wang, J. Fan, Q. Fang, Microfluidic chip-based analytical system for rapid screening of photocatalysts, *Talanta* 116 (2013) 946–950.
- M.R. Prairie, L.R. Evans, B.M. Stange, S.L. Martinez, An investigation of titanium dioxide photocatalysis for the treatment of water contaminated with metals and organic chemicals, *Environ. Sci. Technol.* 27 (9) (1993) 1776–1782.
- H. Jayamohan, Y.R. Smith, B.K. Gale, M. Misra, S.K. Mohanty, Platinum functionalized titania nanotube array sensor for detection of trichloroethylene in water, in: *Sensors*, 2013 IEEE, IEEE, 2013, pp. 1–4.
- Y.-Y. Song, F. Schmidt-Stein, S. Bauer, P. Schmuki, Amphiphilic TiO₂ nanotube arrays: an actively controllable drug delivery system, *J. Am. Chem. Soc.* 131 (12) (2009) 4230–4232.
- Y.R. Smith, R.S. Ray, K. Carlson, B. Sarma, M. Misra, Self-ordered titanium dioxide nanotube arrays: anodic synthesis and their photo/electro-catalytic applications, *Materials* 6 (7) (2013) 2892–2957.
- J.M. Macak, M. Zlamal, J. Krysa, P. Schmuki, Self-organized TiO₂ nanotube layers as highly efficient photocatalysts, *Small* 3 (2) (2007) 300–304.
- H. Lindstrom, R. Wootton, A. Iles, High surface area titania photocatalytic microfluidic reactors, *AIChE J.* 53 (3) (2007) 695–702.
- D. Daniel, I.G. Gutz, Microfluidic cell with a TiO₂-modified gold electrode irradiated by an UV-LED for in situ photocatalytic decomposition of organic matter and its potentiality for voltammetric analysis of metal ions, *Electrochim. Commun.* 9 (3) (2007) 522–528.
- N. Tsuchiya, K. Kuwabara, A. Hidaka, K. Oda, K. Katayama, Reaction kinetics of dye decomposition processes monitored inside a photocatalytic microreactor, *Phys. Chem. Chem. Phys.* 14 (14) (2012) 4734–4741.
- L. Li, R. Chen, X. Zhu, H. Wang, Y. Wang, Q. Liao, D. Wang, Optofluidic microreactors with TiO₂-coated fiberglass, *ACS Appl. Mater. Interfaces* 5 (23) (2013) 12548–12553.
- G. Takei, T. Kitamori, H.-B. Kim, Photocatalytic redox-combined synthesis of L-pipeolinic acid with a titania-modified microchannel chip, *Catal. Commun.* 6 (5) (2005) 357–360.
- H. Aran, D. Salomon, T. Rijnarts, G. Mul, M. Wessling, R. Lammertink, Porous photocatalytic membrane microreactor (P2M2): a new reactor concept for photochemistry, *J. Photochem. Photobiol. A: Chem.* 225 (1) (2011) 36–41.
- D.C. Duffy, J.C. McDonald, O.J. Schueller, G.M. Whitesides, Rapid prototyping of microfluidic systems in poly(dimethylsiloxane), *Anal. Chem.* 70 (23) (1998) 4974–4984.
- J. Kim, R. Surapaneni, B.K. Gale, Rapid prototyping of microfluidic systems using a PDMS/polymer tape composite, *Lab Chip* 9 (9) (2009) 1290–1293.
- E. Sollier, C. Murray, P. Maoddi, D. Di Carlo, Rapid prototyping polymers for microfluidic devices and high pressure injections, *Lab Chip* 11 (22) (2011) 3752–3765.
- H.T. Chang, N.-M. Wu, F. Zhu, A kinetic model for photocatalytic degradation of organic contaminants in a thin-film TiO₂ catalyst, *Water Res.* 34 (2) (2000) 407–416.
- M. Dijkstra, H. Panneman, J. Winkelmann, J. Kelly, A. Beenackers, Modeling the photocatalytic degradation of formic acid in a reactor with immobilized catalyst, *Chem. Eng. Sci.* 57 (22) (2002) 4895–4907.
- N. Daneshvar, M. Rabbani, N. Modirshahla, M. Behnajady, Kinetic modeling of photocatalytic degradation of Acid Red 27 in UV/TiO₂ process, *J. Photochem. Photobiol. A: Chem.* 168 (1) (2004) 39–45.
- H. Yatmaz, A. Akyol, M. Bayramoglu, Kinetics of the photocatalytic decolorization of an azo reactive dye in aqueous ZnO suspensions, *Ind. Eng. Chem. Res.* 43 (19) (2004) 6035–6039.
- Y.R. Smith, R. Gakhar, A. Merwin, S.K. Mohanty, D. Chidambaram, M. Misra, Anodic titania nanotube arrays sensitized with Mn- or Co-doped CdS nanocrystals, *Electrochim. Acta* 135 (2014) 503–512.
- S.K. Mohapatra, M. Misra, V.K. Mahajan, K.S. Raja, Design of a highly efficient photoelectrolytic cell for hydrogen generation by water splitting: application of TiO_{2-x}C_x nanotubes as a photoanode and Pt/TiO₂ nanotubes as a cathode, *J. Phys. Chem. C* 111 (24) (2007) 8677–8685.
- G.P. Smestad, M. Gratzel, Demonstrating electron transfer and nanotechnology: a natural dye-sensitized nanocrystalline energy converter, *J. Chem. Educ.* 75 (6) (1998) 752.

[30] Y. Xia, G.M. Whitesides, Soft lithography, *Annu. Rev. Mater. Sci.* 28 (1) (1998) 153–184.

[31] M.A. Eddings, M.A. Johnson, B.K. Gale, Determining the optimal PDMS–PDMS bonding technique for microfluidic devices, *J. Micromech. Microeng.* 18 (6) (2008) 067001.

[32] A. Houas, H. Lachheb, M. Ksibi, E. Elaloui, C. Guillard, J.-M. Herrmann, Photocatalytic degradation pathway of methylene blue in water, *Appl. Catal. B: Environ.* 31 (2) (2001) 145–157.

[33] K. Rajeshwar, M. Osugi, W. Chanmanee, C. Chenthamarakshan, M. Zanoni, P. Kajitvichyanukul, R. Krishnan-Ayer, Heterogeneous photocatalytic treatment of organic dyes in air and aqueous media, *J. Photochem. Photobiol. C: Photochem. Rev.* 9 (4) (2008) 171–192.

[34] M. Resende, P. Vieira, R. Sousa Jr., R. Giordano, R. Giordano, Estimation of mass transfer parameters in a Taylor–Couette–Poiseuille heterogeneous reactor, *Braz. J. Chem. Eng.* 21 (2) (2004) 175–184.

[35] H.-F. Zhuang, C.-J. Lin, Y.-K. Lai, L. Sun, J. Li, Some critical structure factors of titanium oxide nanotube array in its photocatalytic activity, *Environ. Sci. Technol.* 41 (13) (2007) 4735–4740.

[36] J. Augustynski, The role of the surface intermediates in the photoelectrochemical behaviour of anatase and rutile TiO_2 , *Electrochim. Acta* 38 (1) (1993) 43–46.

[37] R. Beranek, H. Tsuchiya, T. Sugishima, J. Macak, L. Taveira, S. Fujimoto, H. Kisch, P. Schmuki, Enhancement and limits of the photoelectrochemical response from anodic TiO_2 nanotubes, *Appl. Phys. Lett.* 87 (24) (2005) 243114.

[38] Y.R. Smith, A. Kar, V. Subramanian, Investigation of physicochemical parameters that influence photocatalytic degradation of methyl orange over TiO_2 nanotubes, *Ind. Eng. Chem. Res.* 48 (23) (2009) 10268–10276.

[39] T. Zhang, T. Oyama, A. Aoshima, H. Hidaka, J. Zhao, N. Serpone, Photooxidative n-demethylation of methylene blue in aqueous TiO_2 dispersions under UV irradiation, *J. Photochem. Photobiol. A: Chem.* 140 (2) (2001) 163–172.

[40] Y.R. Smith, B. Sarma, S.K. Mohanty, M. Misra, Light-assisted anodized TiO_2 nanotube arrays, *ACS Appl. Mater. Interfaces* 4 (11) (2012) 5883–5890.

[41] Y.-C. Nah, I. Paramasivam, P. Schmuki, Doped TiO_2 and TiO_2 nanotubes: synthesis and applications, *ChemPhysChem* 11 (13) (2010) 2698–2713.

[42] S. Kim, W. Choi, Visible-light-induced photocatalytic degradation of 4-chlorophenol and phenolic compounds in aqueous suspension of pure titania: demonstrating the existence of a surface-complex-mediated path, *J. Phys. Chem. B* 109 (11) (2005) 5143–5149.

[43] T. Wu, G. Liu, J. Zhao, H. Hidaka, N. Serpone, Evidence for H_2O_2 generation during the TiO_2 -assisted photodegradation of dyes in aqueous dispersions under visible light illumination, *J. Phys. Chem. B* 103 (23) (1999) 4862–4867.

[44] V. Subramanian, P.V. Kamat, E.E. Wolf, Mass-transfer and kinetic studies during the photocatalytic degradation of an azo dye on optically transparent electrode thin film, *Ind. Eng. Chem. Res.* 42 (10) (2003) 2131–2138.

[45] L.F. Moody, Friction factors for pipe flow, *Trans. ASME* 66 (8) (1944) 671–684.

[46] R. Jaeger, J. Ren, Y. Xie, S. Sundararajan, M.G. Olsen, B. Ganapathysubramanian, Nanoscale surface roughness affects low Reynolds number flow: experiments and modeling, *Appl. Phys. Lett.* 101 (18) (2012) 184102.

[47] J. Krýsa, G. Waldner, H. Měšťáková, J. Jirkovský, G. Grabner, Photocatalytic degradation of model organic pollutants on an immobilized particulate TiO_2 layer: roles of adsorption processes and mechanistic complexity, *Appl. Catal. B: Environ.* 64 (3) (2006) 290–301.

[48] S.-Z. Chu, S. Inoue, K. Wada, S. Hishita, K. Kurashima, Self-organized nanoporous anodic titania films and ordered titania nanodots/nanorods on glass, *Adv. Funct. Mater.* 15 (8) (2005) 1343–1349.

[49] V. Swaminathan, R. Tchao, S. Jonnalagadda, Physical characterization of thin semi-porous poly(L-lactic acid)/poly(ethylene glycol) membranes for tissue engineering, *J. Biomater. Sci. Polym. Ed.* 18 (10) (2007) 1321–1333.

[50] C.S. Turchi, D.F. Ollis, Mixed reactant photocatalysis: intermediates and mutual rate inhibition, *J. Catal.* 119 (2) (1989) 483–496.

[51] D.F. Ollis, H. Al-Ekabi, Photocatalytic purification and treatment of water and air, in: *Proceedings of the 1st International Conference on TiO_2 Photocatalytic Purification and Treatment of Water and Air*, 8–13 November 1992, London, Ontario, Canada, Elsevier Science Ltd, 1993.

[52] A. Fujishima, T.N. Rao, D.A. Tryk, Titanium dioxide photocatalysis, *J. Photochem. Photobiol. C: Photochem. Rev.* 1 (1) (2000) 1–21.

[53] Y.S. Sohn, Y.R. Smith, M. Misra, V. Subramanian, Electrochemically assisted photocatalytic degradation of methyl orange using anodized titanium dioxide nanotubes, *Appl. Catal. B: Environ.* 84 (3) (2008) 372–378.

[54] Y. Kikuchi, K. Sunada, T. Iyoda, K. Hashimoto, A. Fujishima, Photocatalytic bactericidal effect of TiO_2 thin films: dynamic view of the active oxygen species responsible for the effect, *J. Photochem. Photobiol. A: Chem.* 106 (1) (1997) 51–56.

[55] T. Tatsuma, S.-i. Tachibana, T. Miwa, D.A. Tryk, A. Fujishima, Remote bleaching of methylene blue by UV-irradiated TiO_2 in the gas phase, *J. Phys. Chem. B* 103 (38) (1999) 8033–8035.

[56] R.C. Pena, J. Gamboa, M. Bertotti, T.R. Paixao, Studies on the electrocatalytic reduction of hydrogen peroxide on a glassy carbon electrode modified with a ruthenium oxide hexacyanoferrate film, *Int. J. Electrochem. Sci.* 6 (2) (2011) 394.

[57] T.M. Squires, S.R. Quake, Microfluidics: fluid physics at the nanoliter scale, *Rev. Mod. Phys.* 77 (3) (2005) 977.

[58] R.B. Bird, W.E. Stewart, E.N. Lightfoot, *Transport Phenomena*, John Wiley & Sons, 2007.

[59] K.S. Elvira, X.C. i Solvas, R.C. Wootton, The past, present and potential for microfluidic reactor technology in chemical synthesis, *Nat. Chem.* 5 (11) (2013) 905–915.